AIAA SPACE 2009 Conference & Exposition
14 - 17 September 2009, Pasadena, California

AIAA 2009-6734

AIAA SPACE 2009 Conference & Exposition
14-17 September 2009, Pasadena, California

AIAA-2009-6734

Optimizing Electrodynamic Tether System Performance

Keith R P. Fuhrhop*
Northrop Grumman, Redondo Beach, CA., 90278

and

Brian E. Gilchrist †
University of Michigan, Ann Arbor, MI., 48109

A time-averaged electrodynamic tether (EDT) system simulation tool has been developed and used to conduct studies of tether performance under varying conditions. The studies included evaluating passive end-body electron collection and active ion emission approaches, a comparison of active electron emission technologies (hollow-cathode, electron field emission, hot cathode), adjustment of bare conductor versus insulated tether lengths, boosting and de-boosting conditions, and other various system element configurations. The study results indicate that in many cases bare tether anodes provide optimal electron collection. In addition, it was shown that while hollow cathodes may be the best active electron emission technique, field emitter arrays result in less than 1% difference in average system thrusting and use no consumables. This is based on the assumption that multi-amp field emitter arrays can be ultimately fabricated and qualified for space.

Three case-studies were performed in order to better understand the trades for performance optimization. The cases were: (1) orbit maintenance of the International Space Station; (2) the use of an EDT system for reboost and deorbit of NASA's GLAST spacecraft; and, (3) operation of the Momentum Exchange Electrodynamic Reboost (MXER) system. From evaluation of these cases, a recommended design "algorithm" is proposed. Case (1) is presented in this paper in its entirety, and cases (2) and (3) are briefly described.

Nomenclature

A	= constant in Richardson Eq. [A/cm^2]	J	= current density [A/m^2]
A_e	= area of emitter [m^2]	k	= Boltzmann's constant in [J/K]
α,β	= Parker Murphy correction factor [ ]	m_e	= mass of electron [kg]
B	= constant in Fowler Nordheim equation [A/V^2]	n_e, n_i	= electron / ion density [particles/m^3]
B_{North}	= magnetic flux density in north direction [T]	ϕ	= work function of element in [eV]
C	= constant in Fowler Nordheim equation [V]	ϕ_o	= Intermediate Potential for Parker Murphy [V]
D	= distance across sheath [m]	ρ	= perveance [pervs]
dl	= unit distance [m]	r_b	= radius of emitter [m]
dF	= force per unit distance [N]	r_s	= Radius of plasma sheath [m]
e,q	= electric charge [C]	SA2d	= 2-d Surface Area [m^2]
ε_o	= permittivity constant [F/m]	T	= temperature [K]
η	= thermionic cathode efficiency (~0.97)	T_e,T_i	= electron / ion Temperature [eV]
F	= electric field in [V/m]	T_o	= energy of emitted electrons [eV]
I_{CL}	= space charge limited current [A]	V	= plasma sheath gap potential [V]
$I_{omle,}$,I_{omli}	= electron/ion Orbital Motion Limited Current [A]	V_p	= Plasma Potential [V]
		V_{emf}	= electro motive force [V]
I_{ram}	= Ram Current [A]	ΔV_{tc}	= potential across the thermionic cathode [V]
I_{the}, I_{thi}	= electron / ion Thermal Current [A]	v_{orb}	= orbital velocity wrt. local plasma [m/s]
I_t	= current in the tether [A]	ω_{ce}, ω_{ce}	= electron / ion cyclotron frequency [Hz]

I. Introduction

Electrodynamic tethers (EDTs) are being considered as a propellantless propulsion technology for spacecraft in low Earth orbit. An orbiting tether system naturally orients along the local vertical due to gravity. Current flowing along the

* Systems Engineer, Aerospace Systems, One Space Park / R5-2281B, AIAA Senior Member
† Full Professor, Electrical Engineering and Atmospheric, Oceanic and Space Sciences, 1301 Beal Ave. / 2240 EECS, AIAA Associate Fellow

tether interacts with the Earth's magnetic field to provide thrustvia the Lorentz force. To produce this current, it is generally thought that electrons are collected on one end of the tether and emitted at the other, using the ionosphere as the path to close the electrical circuit. This paper considers various electron emission methods for this purpose and the relative merits thereof.

There are three electron emission technologies typically considered: hollow cathode (HC) plasma contactors, thermionic cathodes (TCs), and field emitter arrays (FEAs). In addition, there are several passive electron collection mechanisms that can be modeled with relative confidence such as: Orbital Motion Limited Theory, Ion Ram Theory, and Parker Murphy Collection. Considering this technology, system level configurations are then presented below and the relative costs and benefits discussed.

II. Elements of EDT Technology: Active Electron Emission & Passive Current Collection Theory

In order to understand the physical effects involved in the following system simulations, it is necessary to understand the basic mechanisms involved. Three electron emission techniques as well as general space-charge limits are discussed. Following this, the passive current collection mechanisms in a flowing plasma, modeled in the simulations of the paper, are presented.

A. Thermionic Emission

When electrons are emitted into a vacuum by a heated electronic conductor cathode, the emission current density, *J*, increases rapidly with increasing temperature; this is illustrated in Eq. (1), the Richardson−Dushman, or Richardson equation (here we assume typical values - ϕ is approximately 4.54 eV and A ~120 A/cm^2 for tungsten).

$$J = AT^2 e^{-\left(\phi/kT\right)} \qquad (1)$$

$$\Delta V_{tc} = \left[\frac{\eta \cdot I_t}{\rho}\right]^{2/3} \qquad (2)$$

TC electron emission will occur in one of two different modes: temperature limited or space charge limited (SCL) current flow. For temperature limited flow, every electron released from the cathode surface is emitted according to Eq.(1. If the cathode temperature can be increased, additional electrons would be emitted. In SCL electron current flow, there are so many electrons emitted from the cathode that not all are able to escape the near region of the surface due to space charge limits (discussed further below). An external applied bias potential is then required to extract this released thermionic charge. This occurs if an accelerated grid, for example an electron gun, is used. Eq. (2 shows what potential is needed across the grid in order to emit a certain current that has entered the device.[1,2]

B. Field Emission

In field emission cathodes, electrons tunnel through a potential barrier, rather than escaping over it as in thermionic emission or photoemission. Electrons are extracted from the conduction band with a current density given by the Fowler−Nordheim equation (Eq. (3).[3]

$$J = B \cdot F^2 \cdot e^{-C/F} \qquad (3)$$

In the following analysis, typical constants yielded for Spindt-type cathodes include: B = 3.14 x 10^{-7} A/V^2 and C = 771 V. (information c/o Stanford Research Institute). An accelerating structure is typically placed in close proximity with the emitting material. To achieve the high surface electric fields required for field emission, the emitting material might consist of a range of materials from semiconductor fabricated molybdenum tips with integrated gates, to a plate of randomly distributed carbon nanotubes with a separate gate structure suspended above. Close (micron scale) proximity between the emitter and gate, combined with natural or artificial focusing structures efficiently provide the high field strengths required for emission with relatively low applied voltage, and low power.[3]

C. Hollow Cathodes

Hollow cathodes emit ions or electrons by ionizing a consumable gas supply to create a high density plasma plume in contact with the surrounding plasma. One type of hollow cathode consists of a metal tube lined with a barium oxide impregnated insert capped at one end by a plate with a small orifice as seen in Figure 1. Electrons are emitted from the insert by thermionic emission. Propellant gas, typically xenon, flows into the tube and exits, partially ionized, out of the orifice. Electrons flow from the insert region, through the orifice plasma to the conductive ring, or keeper, and other anode surfaces.

In electron emission mode, the ambient plasma is positively biased with respect to the keeper. In the contactor plasma, the electron density is approximately equal to the ion density. The higher energy electrons stream through the slowly expanding ion cloud, while the lower energy electrons are trapped within the cloud by the keeper potential.[4] The high electron velocities lead to electron currents much greater than xenon ion currents. Below the electron emission saturation limit the contactor acts as a bipolar emissive probe. Each outgoing ion generated by an electron allows a certain number of

electrons to be emitted. This number is approximately equal to the square root of the ratio of the ion mass to the electron mass.

The operation of the HC in the electron collection mode is called the plasma contacting (or ignited) operating mode. The "ignited mode" is so termed because it indicates that multi-ampere current levels can be achieved by using the voltage drop at the plasma contactor. This accelerates space plasma electrons which ionize neutral expellant flow from the contactor. If electron collection currents are high and/or ambient electron densities are low, the sheath at which electron current collection is sustained simply expands or shrinks until the required current is collected.

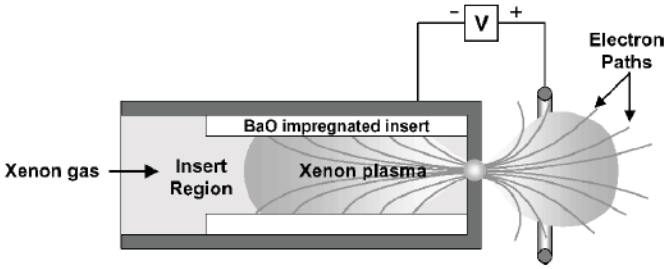

Figure 1: Schematic of a Hollow Cathode System

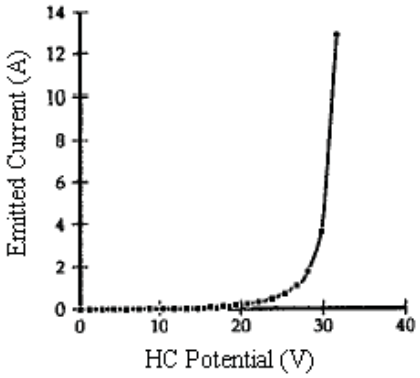

Figure 2: I-V Characteristic curve for a Hollow Cathode

A typical I-V curve for a hollow cathode in the electron collection mode is shown in Figure 2. Given a certain keeper geometry, ion flow rate, and potential, the profile can be determined.[4-6] Much work has been accomplished to create a basic model of the HC.[7,8] This model has been verified for specific cases[9] using various experimental evidence [10,11]

D. Space Charge Limit

In any application where electrons are emitted across a vacuum gap there is a maximum allowable current for a given bias due to the self repulsion of the electron beam. Classical space charge limits depend on current density, gap width, gap potentials, geometry, and initial kinetic energy, shown in the Child–Langmuir Law. Here, the "gap" is an ion-rich plasma sheath transitioning from the background plasma to the spacecraft surface. The presence of ions in the gap (sheath) improves space charge constraints as the ions act to neutralize electron charge. The one-dimensional classical (vacuum gap) Child-Langmuir Law current density limit (in MKS units) is given in Eq.(4, which is multiplied by the area of the planar emitter.[12]

$$I_{CL}(1)=\frac{4\varepsilon_o}{9e}\sqrt{\frac{2}{m_e}}\frac{T_o^{3/2}}{D^2}\left[1+\sqrt{1+\frac{eV}{T_o}}\right]^3 A_e \qquad (4)$$

$$\frac{J_{CL}(3)}{J_{CL}(1)}=\frac{\left[r_b^2+(D/2)^2\right]}{r_b^2}=\left[1+(D/2r_b)^2\right] \qquad (5)$$

Here, we will assume that the plasma sheath gap potential is within a few eV of the local plasma potential, and the sheath width is on the order of a few Debye lengths. These assumptions are consistent with the situation of an electrically isolated (floating) spacecraft or subsystem. The sheath dimension is in general set by the sheath potential, background plasma density, temperature, and geometry. In addition, because of the low electron temperature of ionospheric plasmas in ED tether applications, it is possible to assume $V << T_o$ in Eq. (4.

An enhancement over the 1-d classical Child-Langmuir limit ($T_o = 0$) is possible from a narrow pencil beam (i.e., expansion in two lateral directions) generated by an emitter of radius, r_b, and gap, D, according to the 3-d Space charge limit equation in Eq. (5), where it is assumed that r < D (see Figure 3).[13] It is also noted that multiple pencil beams can be placed in parallel, with each experiencing the enhancement of Eq. (5, provided that the center to center beam spacing is large with respect to D. To estimate a threshold for space charge limited current flow, we will use Eq. (4) with the 3-d addition from Eq. (5). This calculation results in the determination of the current emitted after the space charge limit.

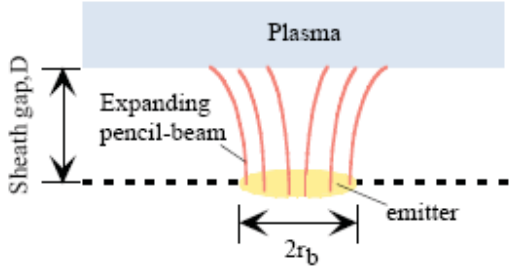

Figure 3: Description of a 3-d expanding pencil beam emitter[11]

Besides transit of the electron beam across an ion-rich sheath, its penetration into and accommodation by the plasma must be considered. The larger the density of the electron beam relative to the background plasma density, the stronger the space charge effects will be even in the plasma. Thus, this

situation will likely be critical for ED tether applications where emitted currents are high and background plasma densities are lower.[14]

E. Orbital Motion Limited Theory

The orbital-motion-limit regime is attained when the cylinder radius is small enough such that that all incoming particle trajectories that are collected are terminated on the cylinder's surface are connected to the background plasma, regardless of their initial angular momentum (i.e., none are connected to another location on the probe's surface). Since, in a quasi-neutral collisionless plasma, the distribution function is conserved along particle orbits, having all "directions of arrival" populated corresponds to an upper limit on the collected current per unit area (not total current).[15]

In an EDT system, the best performance for a given tether mass is for a chosen tether diameter to be smaller than an electron Debye length for typical ionospheric ambient conditions[§] so it would be within the OML regime. The approximation for OML collection will be used as a baseline when comparing the current collection results for various sample tether geometries and sizes. OML current collection by a thin cylinder is given by Eq. (6.[9,15-17]

$$I_{omle,omli} = I_{the,thi}\frac{2}{\sqrt{\pi}}\sqrt{1+\frac{^{(+,-)}V_p}{T_{e,i}}} \quad for\ V_p > 0 \qquad (a)$$

$$I_{rtd} = I_{the}\exp\left(\frac{V_p}{T_e}\right) for\ V_p < 0 \qquad (b) \qquad (6)$$

In these equations there are two distinct regions of OML collection defined as I_{omle} and I_{omli}. When the potential of the collecting body with respect to the plasma potential, $V - V_p$, is negative, ions are collected according to Eq. (6a (I_{omli}) and electrons are collected according to the retardation regime equation of Eq. (6b (I_{omle}). The converse is true when $V - V_p$ is positive. In Eq. (6a and Eq. (6b, $I_{the,thi}$ is the electron and ion thermal current, and represents the quantity of electrons or ions that randomly cross a given area per unit time.

It has been experimentally shown that flowing plasmas yield enhanced current collection compared to what OML theory predicts.[9] This phenomenon is presently being investigated through recent work, and is not fully understood. As a result, for the purposes of simulation of tether current collection in this paper, the non-flowing plasma theory will be applied as a conservative estimate.

F. Parker Murphy Equation (Flowing Plasma)

Electron current collection by a biased conducting sphere, in a non-flowing plasma, is modeled using the Parker-Murphy equation.[18] This equation has been adapted for flowing plasma situations. For a flowing plasma, different effects occur when $V - V_p$ is biased positive or negative. The corrected version of the Parker-Murphy Equation for electron collection (accounting for a flowing plasma) is based on mission data from the TSS-1R mission.[19] These electron collection equations shown in Eq. (7 and Eq. (8, are used in the simulations of this paper. Here, ϕ_o is an intermediate potential used for the Parker Murphy Equation. I_o is the product of the electron thermal current and the 2-d surface area projection of the front and back of the collecting sphere, $2\cdot\pi\cdot r_s^2$. The electron gyro-frequency[**] is ω_{ce}, and α and β (found to be 2.5 & 0.52) are the corrections based on experimental data from of Thompson et al..[9,19]

$$\phi_o = \frac{m_e\cdot {\omega_{ce}}^2 {r_s}^2}{8\cdot q} \qquad (7)$$

$$I_e = \alpha\cdot I_o\cdot\left[1+\left(\frac{V_p}{\phi_o}\right)^{\beta}\right] \qquad (8)$$

Based on the TSS-1R results it is estimated that there is an overall enhancement above the original Parker Murphy collection estimate by a factor of ~2.5. When accounting for plasma flow effects for a positively biased conducting body, many interesting phenomena can be seen. During the TSS-1R mission, when the satellite body exceeded the ram kinetic energy of the ambient plasma[††], a non-uniform distribution of 'suprathermal' electrons appeared on the surface.[20] In addition, magnetic perturbations were detected which show indications of anisotropic current collections due to local cross field transport.[21] It has been initially predicted using TSS-1R data,[22] and then experimentally verified, that one of the causes of the increased current collection over that of Parker-Murphy is due to the ExB drift into the collecting sheath.[23] Other possible reasons have been shown in Particle-In-Cell (PIC) simulations, which predict electron heating and acceleration due

---

[§] Typical ionospheric conditions in the from 200 to 2000 km altitude range , have a T_e ranging from 0.1 eV to 0.35 eV, and n_e ranging from 10^{10} m^{-3} to 10^{12} m^{-3} .

[**] The electron and ion gyro-frequencies are defined as $\omega_{ce,ci} = \frac{q\cdot B}{m_{e,i}}$.

[††] Or when $\frac{1}{2}mv_{orb}^2 > T_e$

to instabilities generated by ion reflection from the sheath potential barrier.[24] Work still remains concerning the understanding of the comprehensive interactions involving all reasons presented, as well as further experimental verification.

G. Ion Ram Collection (Flowing Plasma)

When the conducting body is negatively biased with respect to the plasma and traveling above the ion thermal velocity, there are additional collection mechanisms at work. For typical Low Earth Orbits (LEOs), between 200 km and 2000 km[25], the velocities in an inertial reference frame range from 7.8 km/s to 6.9 km/s for a circular orbit and the atmospheric molecular weights range from 25.0 amu (O^+, O_2^+, & NO^+) to 1.2 amu (mostly H^+), respectively[26-,28]. Assuming that the electron and ion temperatures range from ~0.1 eV to 0.35 eV, the resulting ion velocity ranges from 875 m/s to 4.0 km/s from 200 km to 2000 km altitude, respectively. The electrons are traveling at approximately 188 km/s throughout LEO. This means that the orbiting body is traveling faster than the ions and slower than the electrons, or at a mesosonic speed. This results in a unique phenomenon whereby the orbiting body 'rams' through the surrounding ions in the plasma creating a beam-like effect in the reference frame of the orbiting body.

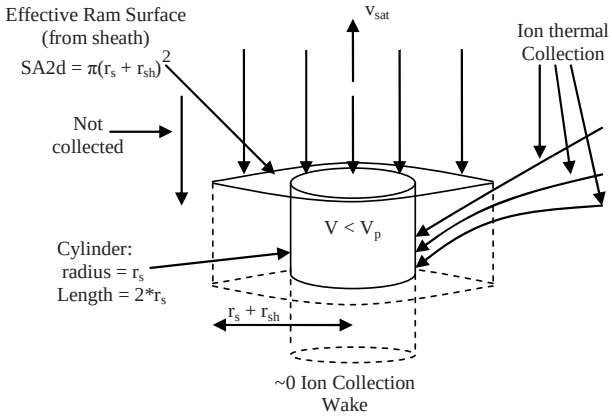

Figure 4: Schematic of the ion collection process

$$I_{ram} = SA2d \cdot n_i \cdot v_{orb} \cdot q \quad \textbf{(9)}$$

Assuming cold ions, the ram current is the total number of ions that impact the ram surface, which can be seen in Eq.(9. This is effectively thermal current collection across a virtual 2-D surface area that grows according to the sheath size. As the ion thermal motion approaches the orbital velocity it should be noted that it is more appropriate to consider the ion motion as a 'drifting maxwellian'. It is also important to note that this is a thin sheath regime, as explained earlier in this section, where all the current that enters the sheath is collected.[29] This implies that the ion thermal collection still occurs across the sheath along the side but not on the wake side. These effects can be seen in Figure 4. A cylinder is used to show the added thermal collection effects that are not due to the ram collection (as opposed to a sphere which would be all ram current collection).

III. ED Tethers: System Integration & Analysis

There are multiple parameters that can be varied in an EDT system to observe changes in performance. Examples include tether resistance, electron density, high voltage power supply (HVPS) power, and electron emitter. EDT system design can involve optimization for boost time, power efficiency, and/or system mass. It is also useful to know what the optimal bare tether length and geometry is for a given mission when designing the system.

This section serves to identify and better describe and understand how elements of an EDT system can impact performance under varying circumstances in boosting and de-boosting scenarios with an emphasis to EDT system design. Based on this, for example, methods can be tested to determine the optimized bare tether amount for a given system.

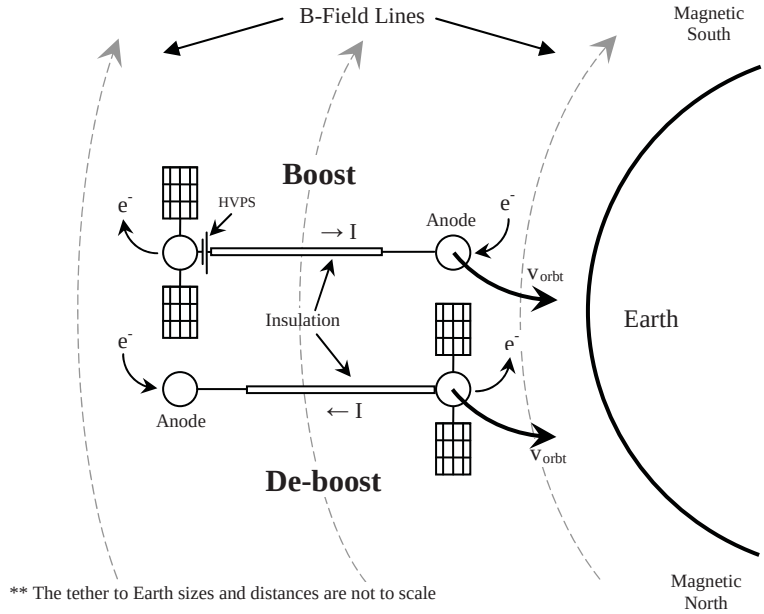

Figure 5: Illustration of the EDT concept

A. Tether Fundamentals

A tether EMF is generated by Eq. (10) as the satellite orbits the Earth. In self-powered mode (de-orbit mode) this EMF can be utilized by the tether system to perform various functions: charge batteries, emit electrons at the emitting end, and drive current through the tether. In boost mode, on-board power supplies must overcome this motional EMF to provide

bias for current collection, electron emission, and tether resistive losses. The physical orientation of a boost and de-boost EDT scenario can be seen in Figure 5.

$$V_{emf} = \left(v_{orb} \times B_{North}\right) \cdot dl \qquad (10)$$

$$dF = dl \cdot I_t \times B_{North} \qquad (11)$$

Take, for example, the NASA ProSEDS mission. The Earth's magnetic field is approximately 0.18 – 0.32 gauss in LEO, and the orbital velocity with respect to the local plasma is about 7500 m/s at 300-km altitude. This results in a V_{emf} of a range of 35 – 250 V/km along the length of the tether (The ProSEDS conducting tether was 5 km long). This established EMF dictates the potential difference across the bare tether which controls where electrons are collected and or repelled. Here, a de-boost tether has a setup that allows for electrons to be collected on the positively biased upper section of the bare tether, and returned to the ionosphere at the lower end. This flow of electrons through the length of the tether moving across the Earth's magnetic field creates a force that produces a drag thrust that helps de-orbit the system as given by Eq. (11). The boost mode is similar to the de-orbit mode except for the fact that an HVPS is also inserted in series with the tether and creates a potential difference greater than the V_{emf}. This drives the current the opposite direction, which in turn causes the upper end to be negatively charged, while the lower end is now positively charged. Both boost and de-boost scenarios will be discussed in detail.

B. Configurations

There are three configurations being considered for connecting the electron emitter to the tether circuit as shown in Figure 6. They are identified as: (a) basic grounded-emitter, (b) basic grounded-gate, and (c) series bias - grounded-gate. The grounded-emitter configuration (Figure 6a) effectively isolates the tether and high-voltage power supply (HVPS) circuit from the electron emitter. The electron emitter bias is exclusively set by the 'emitter bias' supply. However, the gate is at a positive potential with respect to the surrounding space plasma that can attract electrons from the plasma drawing current through the power supply. [30, 31]

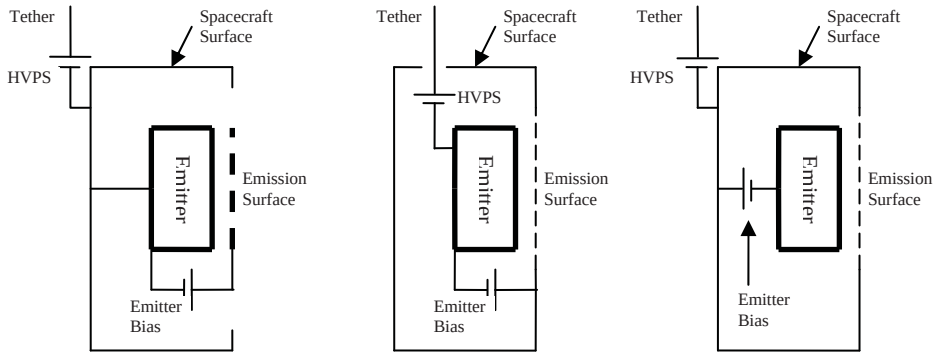

Figure 6: Possible electrical configurations of the electron emitter with the tether and high voltage power supply (HVPS): Grounded tip/emitter (a), grounded-gate (b) and grounded-gate, isolated tether (c) configurations.

A grounded-gate configuration is shown in Figure 6b and c. The grounded-gate configuration allows all external structures, including the field emission gate itself, to be held at the floating potential of the spacecraft, which should minimize the disturbance in the surrounding plasma when the electron emitter is providing all of the tether current. The Figure 6b configuration has the draw-back that if the electron emitter can not provide all of the tether current, then the spacecraft potential will be pulled negative, and possibly substantially negative, through the electron 'emitter bias' supply; adequately protecting the field emitters in that situation is a technical challenge. Our initial assessment, therefore, is that the series bias - grounded-gate configuration in Figure 6c will be the best, most robust option to be utilized for most EDT systems. The drawback to this configuration is that the emitter bias supply must source power, although there is a corresponding reduction in the power provided by the HVPS, and overall power requirements remain unchanged.

When FEAs and TCs are used they have to emit the electrons as close to floating potential as possible in order to be the most efficient.[32] The grounded-gate configurations allow this to occur. The spacecraft surface is at the floating potential in these cases, provided all the current from the tether is being emitted through the emitter without any coming back due to space charge limits. The hollow cathode has a phenomenon called a double sheath which makes the emitted electrons cross two boundary layers: the emitted xenon and the normal plasma sheath. The most accurate way to model this is through (6a). Here the spacecraft body is forced negative by the xenon plasma released from the hollow cathode. Each of these configurations have their own drawbacks and strong points to be considered.

C. Simulation System Setup

A reference EDT system was defined for the majority of the simulations in order to better compare the results. Figure 5 presents sketches of a typical non-rotating boost and de-boost EDT scenario. Each EDT system is based on the

reference tether system scenario and can be seen in Table 1. If certain variables deviate from this reference case, they will be specified in the text.

The baseline tether length was chosen because it was the conductive length for the ProSEDS mission, which also serves as a conservative length for a typical EDT mission.[33] The radius was selected from the TSS-1 mission, since that was the same dimension of the conductive tether (10 strands of 34 AWG wire).[34] The resistance was arbitrarily set to one half of the approximate value of the Hoytether designed for the MXER mission to show what future designs with less resistance might yield.[35] This type of tether has been shown to be a strong design for future missions due to its potential for robust micrometeoroid survivability.[36,37] The radius of the endmass was chosen to be slightly smaller than the TSS-1 mission (0.5 m instead of 0.8) as it was still a reference size. The B-field, electron and ion temperatures, and electron densities were chosen based on typical day time ranges for a 300 km altitude circular orbit.[39,40] The α and β used were the calculated values from the TSS-1R mission.[19] The orbital velocity was acquired by using the typical circular orbit velocity minus the Earths co-rotational velocity. The EMF was found using the given values and Eq. (10. The HVPS power was chosen to be slightly less than the International Space Station (ISS) power as a conservative value for a typical EDT mission.[41]

Tether Length [m]	5000
Tether Resistance [Ω/m]	0.015
B-Field [T] ($\perp$ to L and v_{orb})	2×10^{-5}
Orbital Velocity [m/s]	7000
EMF Potential Difference [V]	700
Tether Radius [mm] (assume wire)	0.6
Electron and Ion Temperature [eV]	0.1
α and β (according to TSS-1R) [ ]	2.5 & 0.52
Spherical Endbody collector Radius [m]	0.5
Load Resistor [Ω]	0
HVPS Power [W]	3000
Electron Emitter	Hollow Cathode
HC Orifice Plasma Density [m^{-3}]	2×10^{20}
HC Plasma Temperature [eV]	3.9
HC Emission Percentage 'f' [%]	100
System Configuration	Grounded tip emitter: Figure 6a

Table 1: Assumptions made for a 'reference case'

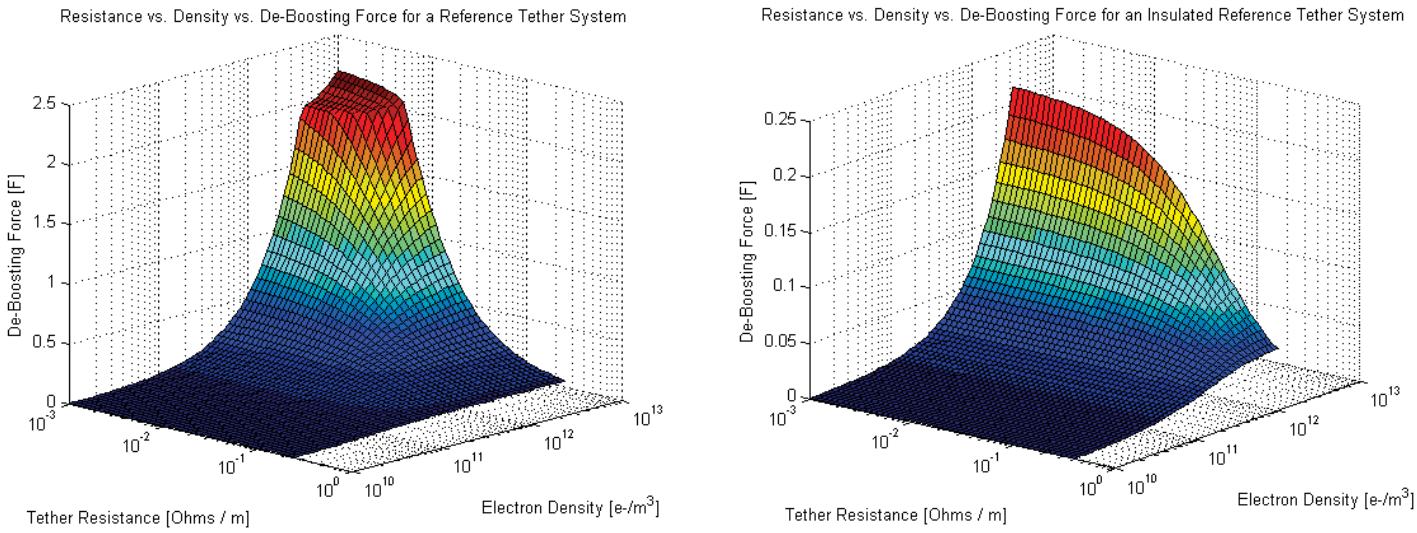

(a) **(b)**

Figure 7: 3d-Plots of the tether resistance versus electron density versus the de-boosting power for (a) a 2500 m bare tether anode and (b) a completely insulated tether.

D. Trade Study Results

The amount of bare tether used in any tether system design will influence the amount of boosting force achievable. It turns out that in most de-boosting scenarios, an almost entirely bare tether will yield the maximum electrodynamic force, compared to one that is insulated. The amount of bare tether must be determined when designing an efficient system for given mission objectives in order to maximize boosting capabilities. It is important to understand how the optimal amount of bare tether changes with the alteration of nearly every system variable.

To begin, a boost case simulation was conducted using approximate day and night electron density conditions of 1×10^{12} and 1×10^{10} $m^{-3,}$ respectively, in order to show the typical extreme conditions encountered throughout an orbit. The

results made it clear that the optimal bare tether distances are quite different between day (~1800 m) and night (~4000 m) conditions.

The boosting impulse was then calculated and found to vary as a function of bare tether length for each of the electron emitters over the course of an entire orbit. The units of impulse were used because they reveal the total amount of force imparted to the system over the course of the entire orbit time. For this particular case, using a total tether length of 5000 m, the optimal bare tether length was ~2500 m when using either the HC or FEA emitters, while with the TC the optimal length was ~1000 m of bare tether.

Using the reference condition and this optimal bare tether amount, tether cases were solved with respect to the electron density, tether resistance, and HVPS. The respective boosting and de-boosting thrust produced by altering these conditions was then plotted. In addition, the insulated tether system and the 2500 m bare tether cases were plotted for the same conditions to compare and contrast the results. It may be useful to refer to Figure 5 to gain a better understanding of the physical orientation in orbit of the EDT system.

i. Deboosting – Vary n_e, R_t

The general trend is for the de-boosting force of the tether system to increase with decreasing tether resistance and increasing ionospheric electron densities. According to Ohm's law, as the tether resistance decreases, the potential from the resistive loss of the tether must diminish as well. The V_{anode} potential is also positive with respect to the plasma potential, resulting in an increase in the electron current. The change in thrust with respect to resistance is seen to drop off more drastically for a system that contains more bare tether. As the bare tether length increases, the de-boosting force increases as well. This is because the increased bare tether surface creates more collection area and more current is collected. In addition, the physical mechanism behind the occurrence starts with the increase in density. This allows more current to be collected for a given surface area, and as can be seen, the more bare the tether, the faster the collection occurs. Figure 7a and Figure 7b detail resistance and electron density effects for a 2500 m bare tether anode and a completely insulated tether.

ii. Boosting: Vary P_{hvps}, n_e, R_t

Figure 8 details the resulting boosting force while varying the HVPS, the tether resistance, and the electron density. As with the de-boosting cases, the system configuration is the reference case, and only the variables mentioned are changing. In addition, the HVPS case is presented in this boosting analysis as it is an essential component to this setup, and not commonly used in a de-boosting case. The resistance per meter is not plotted because it behaves in a manner very similar to the de-boosting case.

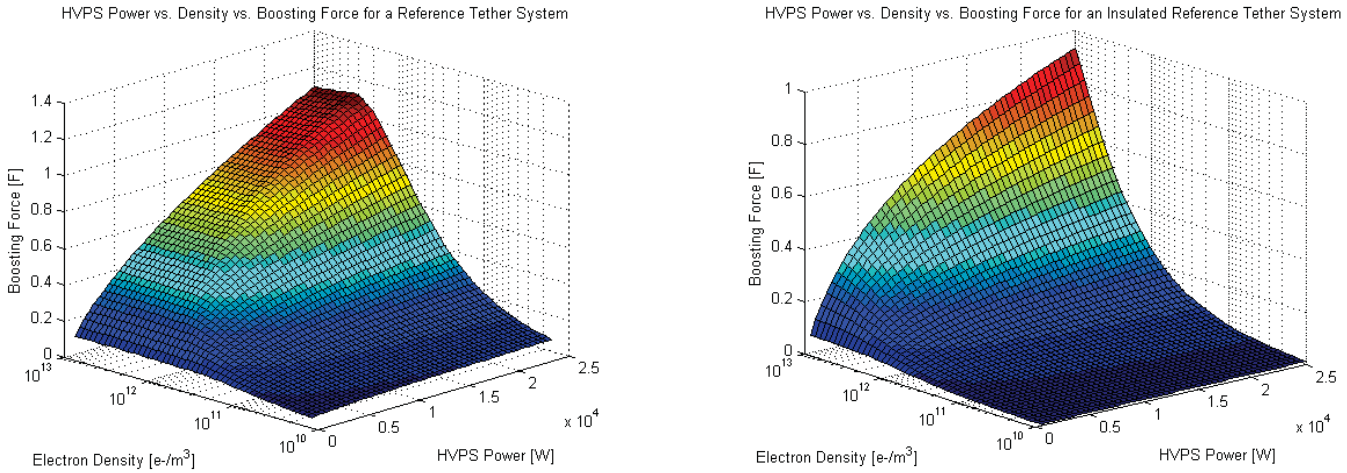

(a) **(b)**

Figure 8: 3d-Plots of the tether resistance versus electron density versus the boosting power for (a) a 2500 m bare tether endbody collector and (b) a completely insulated tether.

In Figure 8, it can be seen that any increase in the HVPS power on an EDT system will result in an increase in the boosting force because of the increase in driving potential. Also, for the same reasons as the de-boosting case, the system always boosts more with increasing electron density and less with increasing tether resistance.

In each of the plots of Figure 8 for the 2500 m bare tether condition, the potential at the endbody collector end of the tether system transitions from positively biased to negatively biased with respect to the plasma. The tether system becomes more positively biased (with respect to the ambient plasma) further up the tether, until it becomes positive again.

This phenomenon can be observed using the current collection and potential profiles for the reference case seen in Figure 9. At 0 m,[‡‡] the endbody collector is negatively biased (-20 V) with respect to the plasma and is thus collecting ions, or a positive current. Around 150 m the V_{emf} drives the potential positive, and the tether begins to collect electrons. This continues until it reaches 2500 m, where it becomes insulated for the remainder of the tether. The I x B · L forces produced by the electron current (orbit raising force) is more than enough to overcome the small forces created by the ion collection (de-orbit force) and as a result yields an overall boosting force for the system in this configuration.

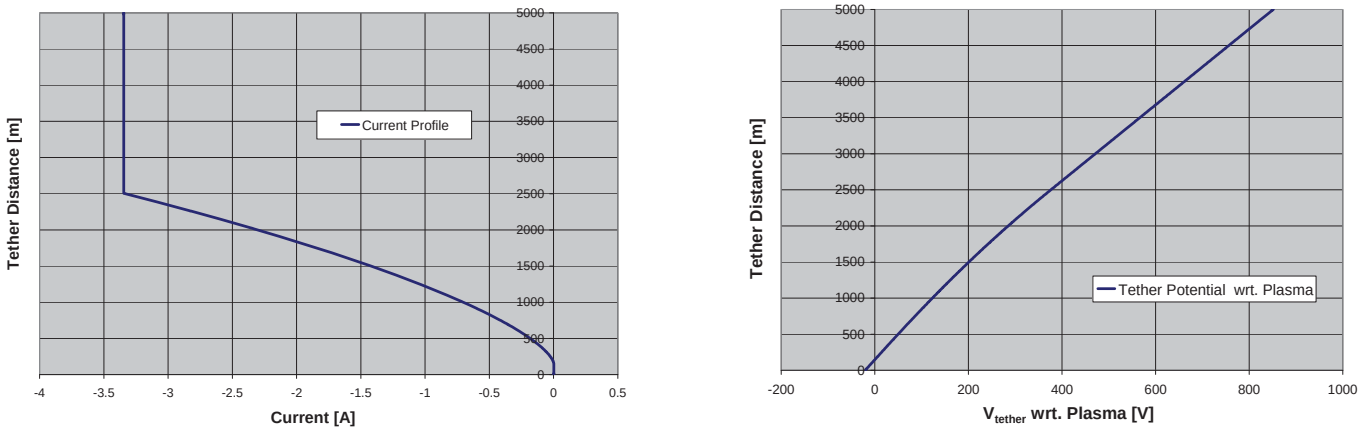

(a) **(b)**

Figure 9: The a) current and b) potential profile of the reference configuration. This shows that the end body is biased negatively for the reference case.

iii. Tether Length Comparison

The next simulation was performed to discover the implications of altering the total length of the tether in the system, while maintaining the same bare fraction. It was observed earlier in this section that there was an optimal length of bare tether for the particular tether system chosen across the three differing emitters for the reference system configuration. In these simulations, the tether is always kept half bare for the HC and FEA cases, and one fifth bare for the TC cases. This is because the maximum force for the reference system using a TC electron emitter was found at this bare tether length. In order to understand the physical effects occurring, the reference system configurations for each emitter will be analyzed with variations in the density and tether resistance for both the boosting and de-boosting cases. In addition, for the boosting case, the high voltage power supply will also be analyzed. An important fact to recall throughout this section is that the V_{emf} increases linearly as the length increases, according to Eq. (10. Also, the basic understanding behind the effects of varying the density, resistance, and P_{HVPS} are explained earlier. This section focuses on discussing the added parameter of increased bare tether length.

a) Hollow Cathode Emitter Results

Figure 10a and Figure 10b show the de-boosting thrust of the reference system configuration as a function of total tether length, with density and tether resistance as parameters. It can be observed in the de-boosting case that the forces vary linearly with increasing tether length for certain situations. As the tether length is initially increased (e.g. 0 – 3 km for $n_e = 1 \times 10^{11}$ m^{-3}), the V_{emf} also increases along with the physical collection area. This allows the tether to collect more current. It can be seen in Figure 10a that as the bare tether length increases, the tether system continuously increases in de-boosting force. The longer tether increases the V_{emf}. As the bare tether length initially increases, this causes the increase in the V_{anode}, and the system collects more current. This causes the V_{tether} to increase because the average current is increasing. As the tether length continues to increase, less current is needed from the spherical endbody collector because of the increased exposed conducting tether. As a result, the V_{anode} reaches a maximum potential point and remains virtually constant, The magnitude of the average tether current does not change much; however, this average is held along a continuously longer length of tether as the total length increases. This produces the linear increase in thrust seen in Figure 10.

[‡‡] For the boosting system, the anode is the lower altitude end.

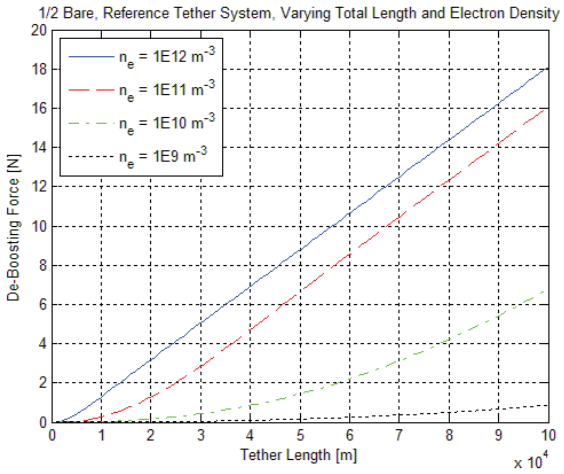

(a)

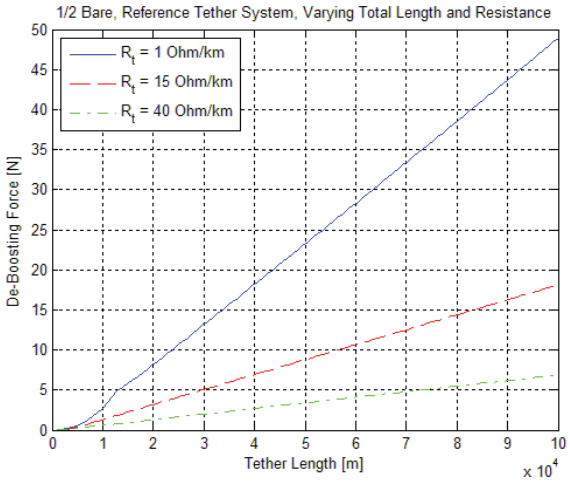

(b)

Figure 10: Hollow cathode de-boosting cases for a reference system configuration (while maintaining a 50% bare tether) varying tether length and comparing (a) density and (b) tether resistance.

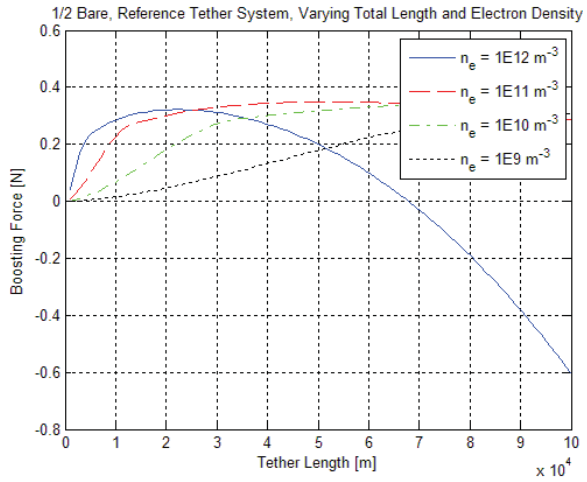

(a)

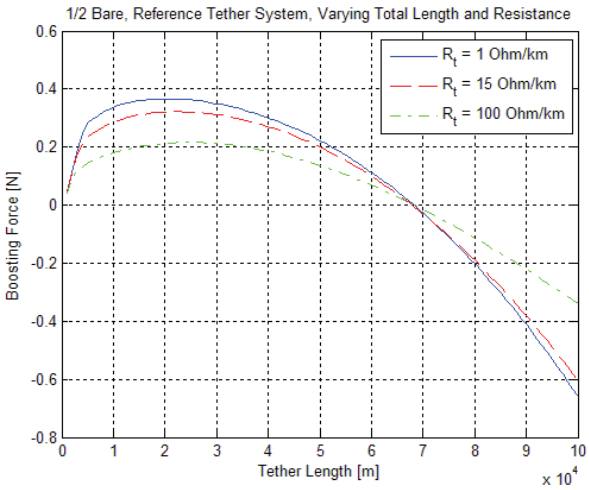

(b)

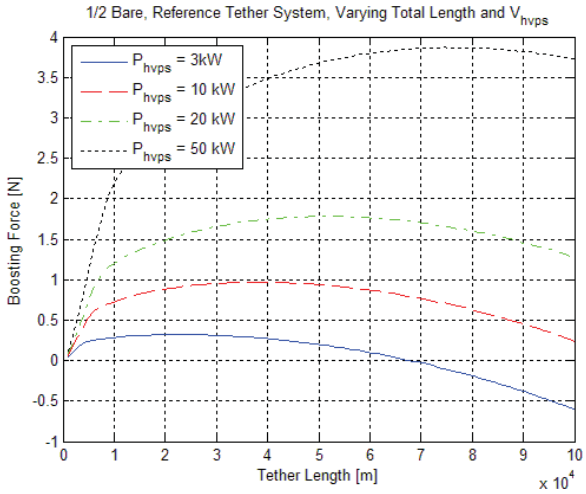

(c)

Figure 11: HC boosting cases varying tether length for (a) density, (b) tether resistance, and (c) the high voltage power supply for a 50% bare tether.

A reference boosting tether system is shown in Figure 11 with density, tether resistance, and P_{HVPS} used as parameters. As before, when the length is increased, the bare tether surface area and the V_{emf} linearly increase. Initially, the increased surface area allows the tether to draw more current. The increase in resistive tether length, as well as the average current, causes the V_{tether} to escalate. In addition, the increase in current also causes the HVPS potential to decrease (in a constant power mode).

Eventually, increasing the bare tether length reaches a point where the total current collection begins to decrease because the tether end potential becomes negative and reduces the net current collected. For this simulation the total HVPS power remains constant. The increase in conductive surface area still allowed for the collected current to increase. The V_{emf} continues to grow with the increasing tether length, and the decreased average current collection causes the V_{HVPS} to increase, since the power supply is constant. These conditions continue until the tether system can no longer maintain a boosting force.

b) Field Emitter Array Results

The same de-boosting system setup was simulated as in the HC case previously discussed, except an FEA was used for electron emission. The particular FEA configuration used here is called the grounded gate, as seen in Figure 6b, and the emitter is allowed to float to whatever potential the end of the system results in with the FEA chosen. The only restriction is that the potential from the gate to the tip cannot exceed ~59 V, since that will damage the emitter. It is assumed that a potential monitor will be used to prevent this from occurring.

As the tether length increases, the de-boosting force results in nearly identical performance to that of the HC data. This is because the physics of the system do not change, only the values associated with the emission. The FEA requires from 0 to ~59 V gate bias, whereas the HC is set at ~27 V for its bias. The maximum current emission capability of the FEA chosen for this analysis was set to a maximum of ~10 A, whereas the HC chosen was set at a maximum of 25 A. This indicates that any time a system requires the electron emitter to release more than its maximum amount of current, it will be capped unless multiple emitters are used. Another limiting factor is the space charge limit, as discussed in Section II-D.

The boosting condition for an identical FEA system was also found to be nearly identical to the HC case. The only difference observed in the boosting case, which was similar to that of the de-boosting case, was that the maximum current emitted by the FEA was also sometimes capped due to the lower maximum current emission. This issue was also addressed by using multiple emitters.

Overall, the FEA biased tether system had nearly identical performance (~1% less) when compared to the HC. The energy required to operate the two systems is also nearly equivalent. The only energy difference would be that which is required to initiate the thermionic process (which begins the electron emission in an HC). In addition, the hollow cathode requires consumables in order to operate, while the FEA does not.

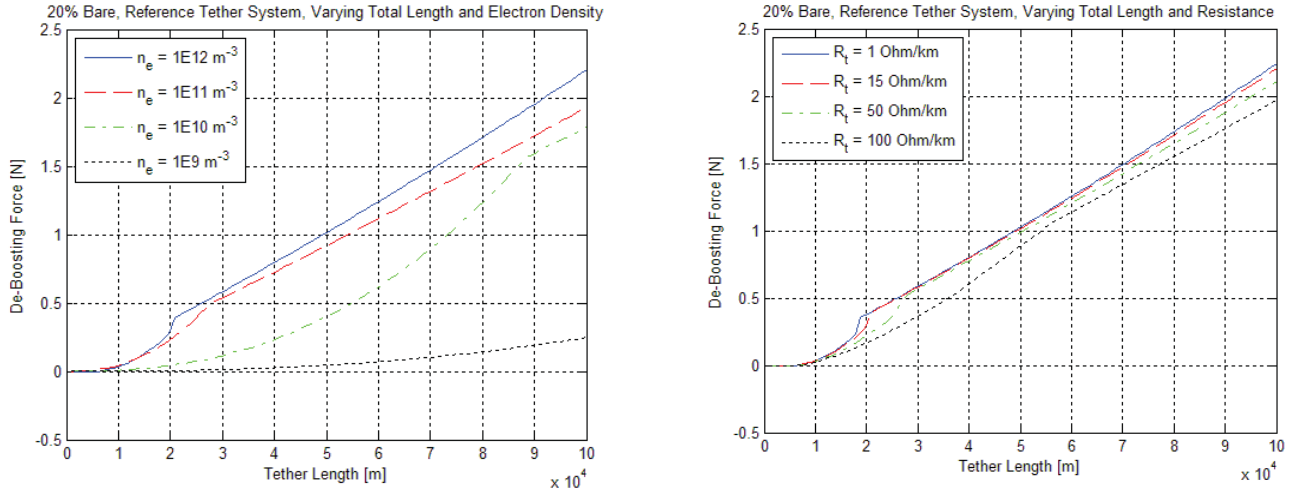

(a) **(b)**

Figure 12: Thermionic cathode de-boosting cases varying tether length for (a) density, and (b) tether resistance for a 20% bare tether.

c) Thermionic Cathode Results

The TC electron emitter case was subjected to the same simulations as the HC and FEA. The major difference for this setup was the proportion of bare tether. It was determined earlier in this section that the optimal amount of bare tether was found to be approximately 20% bare, so this analysis will maintain that amount in the analysis. The system setup configuration is the same as used for the FEA analyses, called the "floating grounded gate", as shown in Figure 6b. Another

differences with the thermionic cathode emitter is the emission potential required to operate it. While the FEA and HCs selected for these analyses requires up to 59 V and ~27 V to operate, the TC selected requires up to 2500 V to operate.

The de-boosting scenario using the TC, as seen in Figure 12, behaves slightly different than the hollow cathode and FEA cases. The non-linear phenomena occurring with the shorter tether lengths are more emphasized for the TCs. The boosting increases until it hits a critical point, at which point it continues a linear de-boosting force increase with the increasing tether length. The potentials and currents involved interact in slightly different ways, however.

As the tether length increases the average current (I_{avg}) increases because the bare collecting surface area and the V_{emf} increases. At smaller tether lengths, under ~5 km, the de-boosting force is shown to be negligible in Figure 12. This is because the potential required to emit the electrons from the TC (which is driven by the V_{emf}) is too great to yield much current. On longer tethers, as the V_{emf} continues to increase, the V_{anode} increases and collects more current until it becomes a positive potential. This increase occurs until the emitter abruptly hits its maximum emission potential of 2500 V. The $V_{cathode}$ now increases in order to compensate for the emitter potential remaining constant. After this point, the same phenomenon occurs as seen with the other two emission devices. The V_{emf} continues to increase and the I_{avg} remains approximately the same. Since the tether length increases, the amount of tether length with this higher current increases. This increases the total thrust.

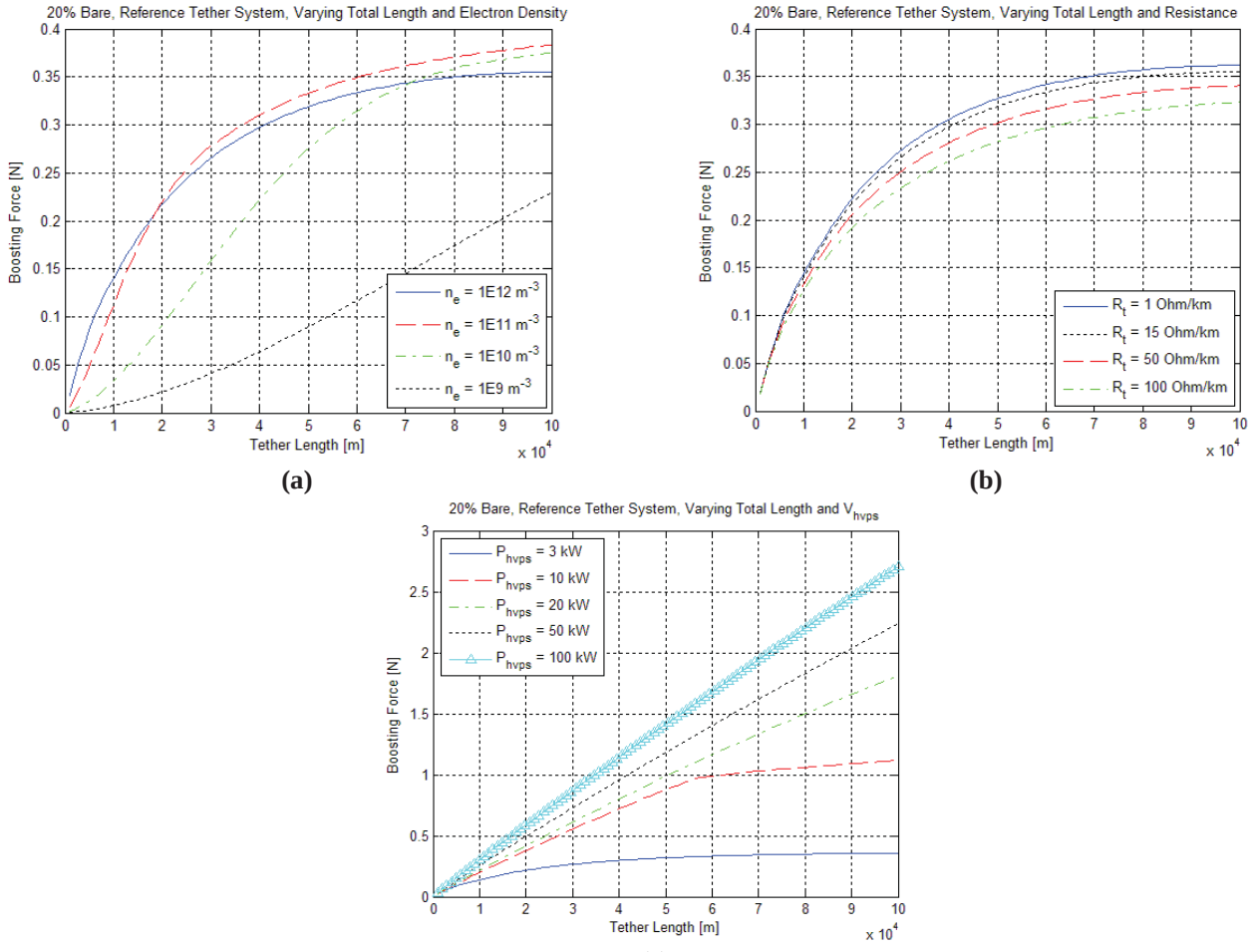

Figure 13: Thermionic cathode boosting cases varying tether length for a 20% bare reference system configuration altering the (a) density, (b) tether resistance, and (c) the high voltage power supply.

The boosting cases for the TC emitter scenarios also behave slightly differently compared to the HC and FEA cases; however, the same mechanisms are at work. Figure 13a, b, and c display the results of the comparative analysis using the 20% bare TC emitter in a reference system configuration.

Overall, the TC power efficiency is lower than the HC and FEA. In addition, the energy required to emit the current is much greater than the other systems. The current emitted is also smaller since common TC emitters used in industry are only capable of emitting 1 to 3 A continuously for long periods of time. The potentials required to operate these emitters

range from 2500 V for 1 A to up to 20,000 V used in some of the larger TC models.[42] There is also energy required to heat the cathode for its operation that must be accounted for. Therefore, a system with an HC or FEA electron emission technology is preferable to that of a TC.

IV. Case Studies

The main reasons for applying EDT technology into current space missions, depending on its application, is because it can significantly reduce the cost and the mass compared to that of conventional propulsive devices. For example, the reduction in consumables alone for drag make-up can save up to a one billion dollars in launch costs over time, as in the case of the International Space Station (ISS), which will be described later. In addition, this section will briefly mention the system design for maintaining the orbit of a large LEO scientific payload, Gamma ray large Area Space Telescope (GLAST), while minimizing mass and adhering to other mission objectives. Finally, EDT thrusting at high ionospheric altitudes is briefly analyzed for the Momentum eXchange Electrodynamic Reboost (MXER) system.[36]

A. System Design Aspects

The mission requirements must first be obtained in order to begin the design process. These include orbital parameters such as the expected mission dates (solar, ionospheric conditions), altitude, inclination, and eccentricity. These values enable the prediction of parameters such as plasma density, electron temperature, magnetic field, etc., which directly determines the forces produced by the system. Next, the constraints of the mission must be determined in order to set boundaries from which to design. Some of these values include available power, system mass, microgravity effects, and mission lifetime. An important new concept will also be explored in this paper involving alternate tether geometries.

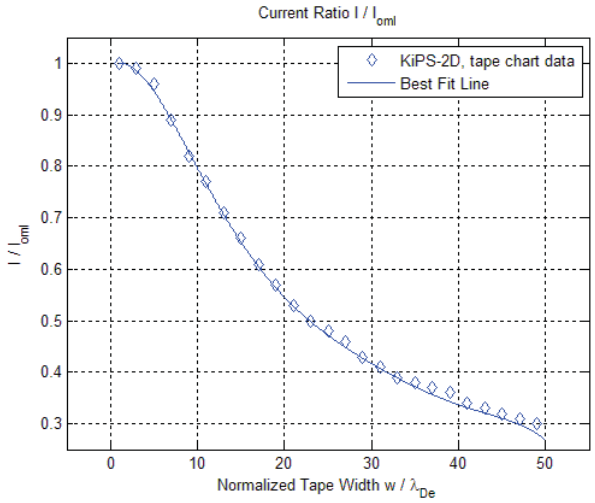

Figure 14: Finding the best fit curve for simulated data describing how the tether width effects current collection that is normalized to OML theory.

For the purposes of this paper the important aspects of modeling tape tethers are presented here. As the width of the tape increases, the electron collection, from the tape surfaces increasingly deviates from OML theory. In order to accurately portray the collection effects, results from a previous experimental test were used.[15] The collection percent of a widening tape changes according to Figure 14, where w is the width of the tape and λ_{De} is the Debye length. The curve presented is only accurate within the range presented. The simulations conducted in this paper all fall within the range of the plot.[44]

Another important factor involving the geometry of the tether is the boosting force of the tether with respect to the force of the drag. A previous experiment determined that the most efficient tether geometry was the 50% porous, holed geometry.[9,45] For the purposes of the case studies, the results of this experiment will be assumed. This assumption is that holed tapes will collect ~81% of the current of an equal width solid tape, but will have 50% of the drag and mass. From this assumption it is implied that an equal mass holed tape will collect ~162% of the current of a solid tape.

	Tape Width [mm]	Endbody Collector Type	Cathode Type	Tape Type	Altitude [km]	Power [kW]	Dates
Range / Types	11, 16, 21, 31, 41	HC Bare Tether Sphere: r = 0.5, 2, 5, 10 m	HC FEA	Solid Holed	350, 450	5, 10, 15	July 1996 (solar max) Dec. 2001 (solar min)

Table 2: The manipulated variables tested by the simulation

B. Case Study: International Space Station (ISS)

The ISS has a great need for inexpensive orbit maintenance and maneuvering. The station maintains an orbit that decays between ~350 and ~450 km over a few years, it needs to be constantly re-boosted. There have already been several investigations to assess the use of tethers on the ISS to account for this decay[41,43,46] as well as other electromagnetic effects.[47,48] This particular study employs unique attributes never before investigated to implement an EDT system for use on

the ISS. Variables such as the tether width, tether porosity, anode type and cathode type will be introduced as new system parameters to be explored. Previous addressed variables such as altitude, system power, and mission date will also be used.

i. Setup

The variable range chosen to be manipulated in this study is detailed in Table 2. It can be seen that many variables are still open to evaluation. Tape widths were chosen at the width Vas et al.[41] analyzed in a previous study, and then increased by increments of 5 and 10 mm. The HC, and a range of conducting sphere endbody collector sizes were investigated in order to determine the optimal electron collection method. The FEA and the HC electron emission cathode technologies were investigated, even though the current emission required is beyond the range of present FEA technology. Thermionic cathodes are not pursued, since they were shown to require excessive power in the previous section. The two tape geometries experimentally investigated, solid and holed, are implemented in this study as well.[9,45] The altitudes to be investigated were found through predicted ISS plans to be within the ranges of 350 and 450 km. The HVPS was stated as being limited at 10 kW by Vas et al..[41] As a result, power levels above and below that were simulated to cover a broader range of possibilities. Finally, since the ISS is a long term mission, it is important to simulate both solar maximum and minimum conditions. The simulations conducted also accurately portray a full day-night cycle of ionospheric conditions by taking a data point each minute over an entire orbit and then averaging the results. These ISS simulations account for the B_x and B_y magnetic fields at the 51.6º inclination at 350 km and 450 km altitude to give a more accurate prediction of the in-plane boosting force.

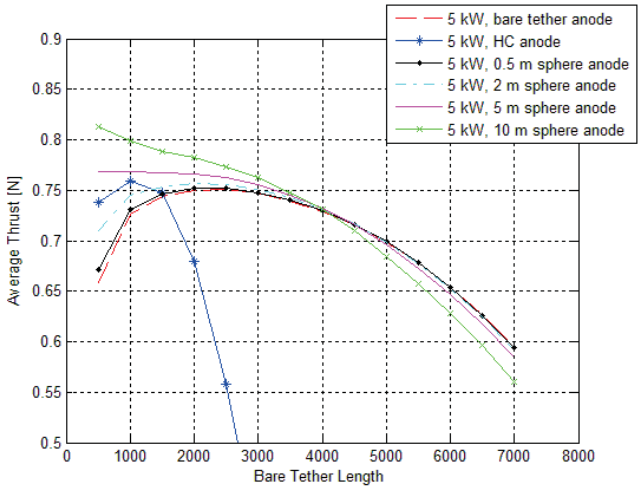

Figure 15: Bare tether length vs. average thrust for a 10 km tether system with an HC e- emitter at 350 km altitude during solar minimum comparing various endbody collectors for a 0.6 mm thickness, 11 mm width tether

ii. Analysis: Trends

As the simulations began, it was observed that the FEA electron emitter produced near identical results to that of the HC electron emitters, as described in the previous section. These emitters each require an equivalent amount of power to operate. As a result, it can be assumed that future runs would behave in the same manner, so further FEA cathode runs were not performed. Also, an important note concerning these simulations was that in order for the HC and FEA to function in the system, it was required that they be large enough to emit all of the current traveling through the tether. As a result of this fact, during the FEA tests (10 kW and above) it was necessary for 2 FEAs, that could each emit 10 A, to be used in order for the system to solve properly. The HC design used for these simulations had a maximum value of 25 A, and only one was required for all the tests presented here.

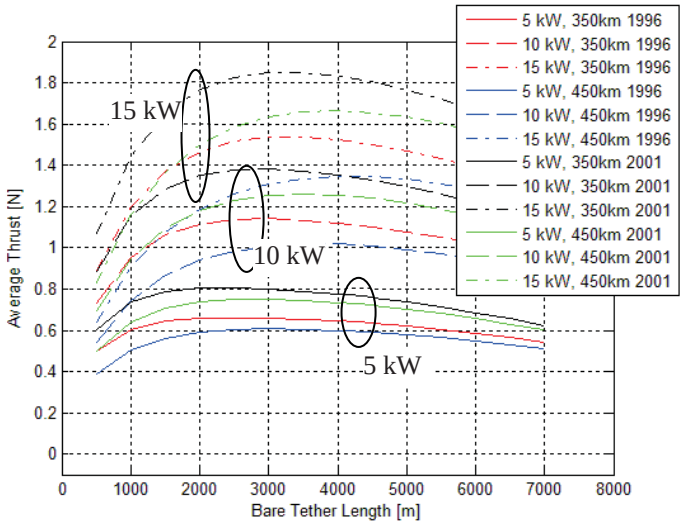

Figure 16: Bare tether length vs. average thrust for a 7 km tether system with an HC e- emitter comparing various dates and altitudes for a 0.6 mm thickness, 11 mm width tether

The first simulation pertains to the endbody collector effects on the system, and can be seen in Figure 15. The bare tether and the various sized spherical endbody collectors have very little affect on the maximum average thrusting point. It took a sphere with a 10 m radius to collect enough current to yield a system boost that surpasses the other endbody collectors, and then by only 0.05 N. In addition, the hollow cathode was found to have a maximum boosting force equivalent to a spherical endbody collector slightly smaller than the 5 m case. The HC, however, resulted in a system that dropped off rapidly as the bare tether length increased. The rapid thrusting drop off by the HC with increasing bare tether length is due to its electron and ion current collection characteristics. In the

case of the bare tether with no spherical endmass or HC, the OML theory collection dictates the rate of electron or ion emission, because it is a thin wire with respect to the Debye length. Since the HC and spherical endbody collectors add complexity and weight to the system, and have minimal effects on the overall results, future analyses were done excluding these cases. In addition, the HC endbody collector limits where the tether's optimal performance would occur to a small bare tether length. As parameters such as the HVPS, altitude, and date change in a mission, the optimal bare tether amount changes. For the ISS, a system must be chosen that performs well under a wide range of orbital and system parameters. The bare tether endbody (anode) electron collector can operate near optimal thrusting performance under a wider range of conditions. For this reason the HC was no longer considered as a potential anode for this system.

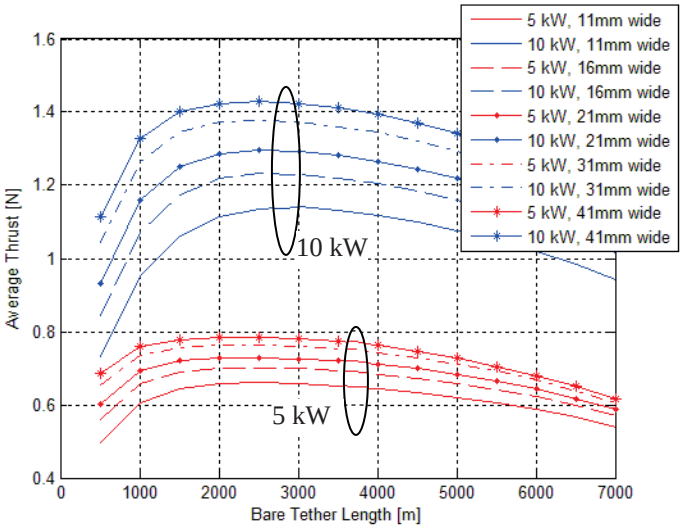

Figure 17: Bare tether length vs. average thrust for a 7 km tether system with an HC e- emitter at 350 km for a 0.6 mm thickness tether comparing various width tethers

In another simulation it is shown from both the 7 km tether case in Figure 16 and the 10 km case that the differences in thrust are 15% between solar maximum and solar minimum cases. Another significant observation shown in Figure 16 is that the optimum bare tether length occurs at nearly the same point despite changes in the altitude and solar cycle point. This trend holds well for the 5 kW system, but varies slightly because the solar cycle has no significant impact on the optimum bare tether length at all powers. This affect likely occurs because despite the overall electron densities being different at various points in the solar cycle, the day to night thrusting relationship is relatively consistent.

The next analysis was performed to compare tethers of different widths. This was conducted for the bare tether at just 5 and 10 kW power supplies because it was shown earlier that larger powers could be extrapolated. The 7 km tether simulation results are seen in Figure 17. These simulations display the fall off in collection efficiency from OML as the width gets larger. The thrust does increase as the width of the tape increases despite the increasing drag. It can be seen that this thrust increase diminishes as the width increases. If the tether continues to become wider, then the increase in drag will more than outweigh the thrust enhancement, and their thrust will begin to drop.

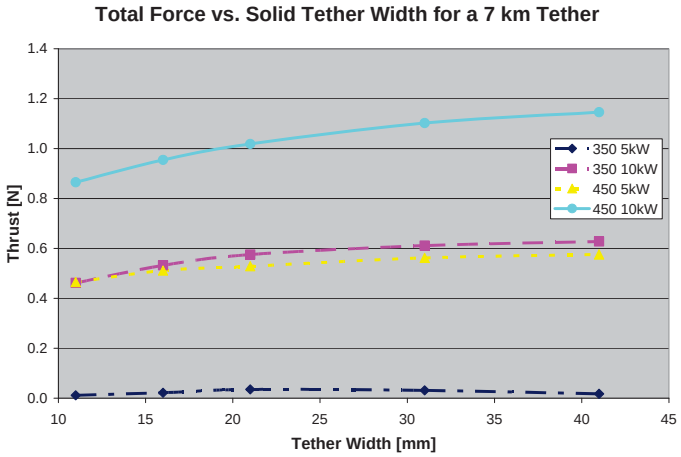

Figure 18: The change in thrust with the change in width for an a) 7 km and a b) 10 km tether system.

iv. Analysis: Optimization Methods

All of the cases simulated thus far can be applied to holed tapes using an approximation. From a previous experiment, it was found that the total current that was collected for normalized potentials $[(V_0 - V_p)/T_e]$ of 50 and 100 were approximately 75% and 81% of the total solid tape collection, respectively.[945] In the ionosphere at the altitudes mentioned, the experiment translates to a tether-to-plasma potential difference of 5 V and 10 V. Since the potentials encountered in a typical EDT system can be up to several kV, depending on the amount exposed and the environmental conditions, this is not a reference value. It does suggest, however, that as the tether to plasma potential increases, the percentage of current collection of holed tapes comes closer to that of solid tapes. For this analysis, the 81% factor was applied as a conservative estimate until more experimentation can be accomplished to verify higher voltage values. This assumption is weak: nevertheless it is the best that can be done given the small amount of experimental and theoretical data.

In order to assess the total amount of system boosting force each respective tether sample results in, the total drag must be accounted for and subtracted out. It was found that for the 350 km altitude simulations, as observed in Figure 18, a maximum value can be discerned. These maximum points at 350 km, 5 kW are ~21 mm and ~16 mm width for the 7 km and 10 km tethers, respectively. A maximum also exists for the 350 km altitude for 10 kW at ~31 mm. The remaining cases

exhibit a similar behavior, where a total thrust maximum value is being approached but not attained. This indicates that tapes of increasing width improve total boosting force only to a point before the drag exceeds the thrusting of the tether. Optimum points will be obtained if even larger width tapes are used, but as will be explained in the next section, wider tethers will be shown to be too massive and far beyond the necessary thrust for a practical system.

The next value to be analyzed is the impact an equal mass OML tether will have on the system analysis. The most current that a tape can collect would be according to OML theory. However, as the tape becomes wider, the electron current collection deviates from this theory according to Figure 14.[15] The tapes are now divided into 10 equal sections which are each small enough to be in the OML regime. These narrower tapes would also have the same V_{emf} across them as the larger width tapes, because they are all in a parallel connection. The resistance for each section, however, will increase by a factor of 10. These results can be seen in Figure 19, which analyzes the 7 km cases for both the solid tapes and the holed tapes. For this case, it is shown that the performance is always significantly better than the single, wider tether, as was predicted by OML theory. In Figure 19, similar color lines are of equivalent mass.

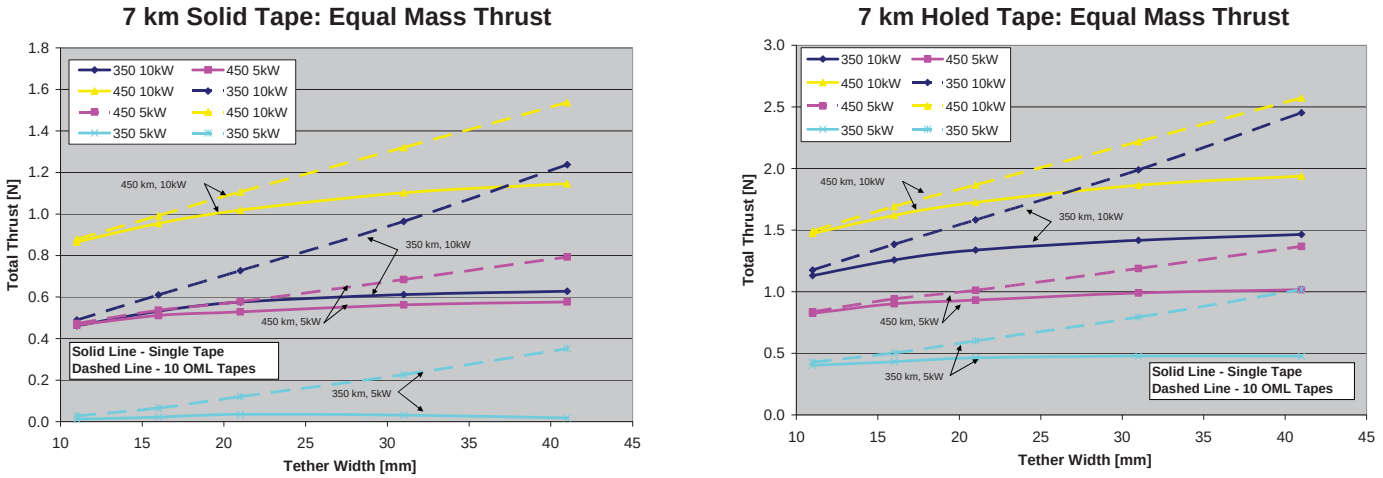

(a) **(b)**

Figure 19: Comparison between a single wide tape tether and a 10 equivalent mass tethers, which are small enough to collect under OML theory at a) 7 km solid, b) 7 km holed tether lengths

iii. Conclusions

Overall, it appears that the highest total thrust results in the 450 km 10 kW system using the 10 km long, 41 mm wide, holed tape, which is bare for 2 km. This system produces a net thrust of 1.9 N (which accounts for the drag of the ISS and the tether). Ideally the best case overall would be to have multiple tether lines, where each individual tether is in the OML regime. This would greatly enhance the performance of all tether widths. The only issue with this is that the tethers would have to be several hundred Debye lengths apart to take full advantage of this fact. In addition, HVPS powers larger than 10 kW would also enhance the system performance, but 10 kW was the design condition limit. Similarly, a longer tether would be better, but is limited at 10 km. A bare tether was used as the electron collection mechanism. For this 10 km system, there would need to be an endbody of ~52 kg, in order to keep the tether taut. If a payload is not on this endbody, then it may be used to contribute toward the electron collection as a conductive body. This would enhance the electron collection and increase the maximum boosting force.

The results here are not as conclusive as they could be. This is due to the fact that more refined questions need to be answered before a total analysis can be conducted. For example, the best case described above tried to yield the highest thrust. This resulted in a system that could produce much more boosting force than was necessary for an orbital maintenance application. A smaller value would save on power consumption as well as system mass, and thus cost. Also, the lifetime of the ISS can affect the width of the tether necessary. Thicker tethers will be required for longer missions. In addition, the available surface area on the ISS, for EDT sub-system will be important. FEAs and multiple strand tethers will require a lot of space in order to operate at their maximum efficiency. These particular design conditions need to be investigated and specified in order to acquire a complete analysis.

C. Additional Case Studies: NASA's Gamma Ray Large Area Space Telescope (GLAST) & Momentum eXchange Electrodynamic Reboost (MXER)

The complete discussion and trade studies completed for the GLAST & MXER case studies are presented elsewhere due to length issues.[9] A summary of the new contributions and analysis is presented here.

i. GLAST

Unique simulations are presented to investigate the issues that were not covered in the initial simulation work by Gilchrist et al..[49] For this case study, the orbit inclination was analyzed at 5˚, instead of 28.5˚ to reduce the time spent in the South Atlantic Anomaly (SAA)[§§]. A more complete simulation using different width porous tethers was also conducted using previous experimental results.[9,45] The most power efficient orbit maintenance scenario was then identified.

The constraints for the simulation of this mission were to test tether lengths of 2, 3, and 5 km; 50% porous aluminum tape widths of 25, 30, and 35 mm wide[***] and 1 mm thick; and tether boosting times of 5, 10, and 20 minutes. The power required to achieve the necessary orbit maintenance for the respective boosting times was then obtained. In addition, the tension due to the gravity gradient force was chosen to be two times the thrust value for dynamic stability. A 30% contingency was then added to account for any discrepancies in the final design.

The results indicate that the optimal boosting design under the given constraints for the GLAST mission would be one that employs a 2 km, 25 mm width porous tether with a 20 minute boost per orbit. The optimum point is not found with the simulations, however as there are limitations beyond the values used. Evidence shows that narrower, shorter tethers that boost for longer periods of time will yield even lighter systems that require less power. The limiting factor on the tether width will be the mission lifetime. Once it becomes too narrow, the chances that a micrometeoroid will sever it will rise sharply. Also, the boosting capability will drop off as the tether becomes shorter until the point where the power to overcome the orbital drag will cause the system weight to be too great. Finally, if the boosting time becomes too great, then the elipticity of the orbit will increase.

ii. MXER

This case study employs the EDT system simulations and techniques developed to identify potential enhancements in the MXER system from that of previous work.[36] The higher altitude environmental conditions are discussed as well as their impact on the system. The MXER system bare tether amount is optimized according to the electron collection device below 2000 km. Finally, various high current HCs are explored in hopes of improving the average thrust above and below 2000 km. A major issue concerning this system is if it can generate enough of an impulse during the perigee of the orbit, where the electron density is the greatest, so it can raise the apogee in a reasonable time frame. The goal of these simulations is to determine if there is a way to enhance the thrusting on MXER such that it can re-boost from post momentum exchange to pre-momentum exchange conditions in a reasonable time frame.

The implications of this work demonstrate that a bare tether anode is the optimal choice for the previously designed MXER system. In addition, the optimal amount of bare tether for this mission has been identified. EDT operations will likely be worthwhile in even higher altitude Earth orbits (for the MXER system) as the electron density does not drop off dramatically enough to disprove further investigation.

V. Conclusion

Hollow cathodes, field emitter arrays, and thermionic cathodes have been evaluated for their actual and predicted effectiveness as electron emitters in an EDT mission. The pros and cons of each individual technology are seen in Table 3. Overall, the TC was found to require too much power, HCs were found to be the most reliable and functional. FEAs were found to be as useful as HCs and not require any consumables, though they are not capable of higher current emissions yet.

Hollow Cathode	Field Emitter Array	Thermionic Cathode
+ Reliable & Proven	- Not Proven Yet	+ Reliable and Proven
+ Robust	- Damageability	+ Robust
+ High Current capable	+ Medium Currents (possibly)	- Low Currents
+ Low Power	+ Medium Power	- High Power
- Consumes Fuel (mass)	+ No Consumables	+ No Consumables
	+ Redundancy	- Requires electron gun

Table 3: Electron emitter comparisons

For the de-boosting cases, the general trend revealed that higher electron densities and lower tether resistances produce the greater forces. In addition, as the tether system increased in bare tether length, from 0 to 2500 m (of a 5000 m

[§§] The South Atlantic Anomaly is the region where Earth's inner van Allen radiation belt makes its closest approach to the planet's surface. The result is that, for a given altitude, the radiation intensity is higher over this region than elsewhere. The SAA is produced by a "dip" in the Earth's magnetic field at that location, caused by the fact that the center of Earth's magnetic field is offset from its geographic center by 450 kilometers [195].

[***] The tether widths of 30 and 35 mm were different than that of the original simulations performed by Gilchrist et al..[49] This is due to the fact that current collection differences between the varying widths are now understood better, and can be accounted for.

tether), the de-boosting force continued to increase as well. Above ~300 Ω/km tether resistance and below ~5 x 10^{10} m^{-3} electron density, the amount of bare tether in the system had negligible impact in the performance (for the particular system setup simulated).

For boosting cases, similar trends were seen for the resistance and the electron density. A small deviation from the de-boosting trend existed for tether resistances and electron densities where the optimal thrusting force changed as the bare tether length increased. There was a point where bare tether length resulted in a decline in performance. This factor depended on the atmospheric conditions and the tether system setup. Also, as the HVPS increased, the resulting boosting force increased no matter what the system setup or atmospheric conditions.

It has been shown throughout this paper that EDT technology can be designed and applied toward nearly all space systems, resulting in some overall benefit. Furthermore, with the development and on-orbit testing of new tether geometries and active electron emission technologies, EDTs may result in significant improvement over conventional propulsion systems.

References

[1] Dobrowolny, M., and Stone, N.H., "A Tecnical Overview of TSS-1: the First Tethered-Satellite System Mission," *Il Nuovo Cimento Della Societa Italiana Di Fisica,* Vol. 17C, No. 1, 1994, pp. 1-12.

[2] Bonifazi, C., Svelto, F., and Sabbagh, J., "TSS Core Equipment. I. - Electrodynamic Package and Rational for Sydtem Electrodynamic Analysis." *Il Nuovo Cimento Della Societa Italiana Di Fisica,* Vol. 17C, No. 1, 1994, pp. 13-47.

[3] Gomer, R., "Field Emission," in AccessScience@Mcgraw-Hill, http://80-www.accessscience.com.proxy.lib.umich.edu/server-java/Arknoid/science/AS/Encyclopedia/2/25/Est_256200_frameset.html, last modified: January 28, 2002.

[4] Parks, D.E., Katz, I., and Buchholtz, B., "Expansion and electron emission characteristics of a hollow-cathode plasma contactor," *Journal of Applied Physics,* Vol. 74, No. 12, 2003, pp. 7094-7100.

[5] Katz, I., Lilley, J. R. Jr., and Greb, A., "Plasma Turbulence Enhanced Current Collection: Results from the Plasma Motor Generator Electrodynamic Tether Flight," *Journal of Geophysical Research,* Vol. 100, No. A2, 1995, pp. 1687-1690.

[6] Katz, I., Anderson, J.R., and Polk, J.E., " One-Dimensional Hollow Cathode Model," *Journal of Propulsion and Power,* Vol. 19, No. 4, 2003, pp. 595-600.

[7] Domonkos, M.T., "Evaluation of Low-Current Orificed Hollow Cathodes," *University of Michigan Ph.D. Dissertation,*1999, pp. 1-173.

[8] Science Applications International Corporation (SAIC), "Chapter 12.3 - Plasma Contactors" *Environment Work Bench User's Reference Manual,* March 2003, pp. 12.11 – 12.23.

[9] Fuhrhop, K., "Theory and Experimental Evaluation of Electrodynamic Tether Systems and Related Technologies," *University of Michigan Ph.D. Dissertation,* 2007, pp. 1-307.

[10] Williams, J.D., and Wilbur, P.J., "Gound Based Tests of Hollow Cathode Plasma Contactors," *3rd International Conference on Tethers in Space - Toward Flight,* AIAA, 1989, pp. 77-87.

[11] Williams, J.D., "An experimental investigation of hollow-cathode-based plasma contactors," *Colorado State University Ph.D. Dissertation,* 1991, pp. 1-125.

[12] Gilchrist, B.E., Johnson, L., and Bilen, S.G., "Space Electrodynamic Tether Propulsion Technology: System Considerations and Future Plans," *AIAA/ASME/SAE/ASEE Joint Propulsion Conference and Exibit,* 1999, pp. 1-8.

[13] Humphries, S., Jr., "Charged Particle Beams," John Wiley & Sons, Inc., Ney York, 1990, pp. 834.

[14] Gilchrist, B.E., Gallimore, A.D., and Jensen, K.L., "Field-Emitter Array Cathodes (FEACs) for Space-Based Applications: An Enabling Technology," Not Published, University of Michigan, 2001.

[15] Choinere, E., "Theory and Experimental Evaluation of a Consistant Steady State Kinetic Model for 2-D Conductive Structures in Ionospheric Plasmas with Application to Bare Electrodynamic Tethers in Space," 2004, pp. 1-313.

[16] Mott-Smith, H.M., and Langmuir, I., "The Theory of Collectors in Gaseous Discharges," *Physical Review*, Vol. 28, 1926, pp. 727-763.

[17] Choiniere, E., Gilchrist, B.E., Bilen, S.G., "Measurement of Cross-Section GeometryEffects on Electron Collection to Long Probes in Mesosonic Flowing Plasmas," *39th AIAA/ASME/SAE/ASEE Joint Propulsion Conference and Exhibit*, AIAA, 2003, pp. 1-13.

[18] Parker, L.W., and Murphy, B.B., "Potential Buildup on an Electron-Emitting Ionospheric Satellite," *Journal of Goephysical Research*, Vol. 72, No. 5, 1967, pp. 1631-1636.

[19] Thompson, D.C., Bonifazi, C., Gilchrist, B.E., "The current-voltage characteristics of a large probe in low Earth orbit: TSS-1R results," *Geophysical Research Letters*, Vol. 25, No. 4, 1998, pp. 413-416.

[20] Winningham, J.D., Stone, N.H., Gurgiolo, C.A., "Suprathermal electrons observed on the TSS-1R satellite," *Geophysical Research Letters*, Vol. 25, No. 4, 1998, pp. 429-432.

[21] Mariani, F., Candidi, M., Orsini, S., "Current Flow Through High-Voltage Sheaths Observer by the TEMAG Experiment During TSS-1R," *Geophysical Research Letters*, Vol. 25, No. 4, 1998, pp. 425-428.

[22] Cooke, D.L., and Katz, I., "TSS-1R electron Currents: Magnetic Limited Collection from a Heated Presheath," *Geophysical Research Letters*, Vol. 25, No. 5, 1998, pp. 753-756.

[23] Gunell, H., Larsson, M., and Brenning, N., "Experiments on anomalous electron currents to apositive probe in a magnetized plasma stream," *Geophysical Research Letters*, Vol. 27, No. 2, 2000, pp. 161-164.

[24] Singh, N., and Leung, W.C., "Numerical Simulation of Plasma Processing Occuring in the Ram Region of the Tethered Satellite," *Geophysical Research Letters*, Vol. 25, No. 5, 1998, pp. 741-744.

[25] Gregory, F.D., "NASA Safety Standard Guidelines and Assessment Procedures for Limiting Orbital Debris," NASA, NSS 1740.14, Washington D.C., 1995.

[26] Bilitza, D., "International Reference Ionosphere 2000," *Radio Science*, Vol. 36, No. 2, 2001, pp. 261-275.

[27] Bilitza, D., "International Reference Ionosphere - Status 1995/96," *Advanced Space Research*, Vol. 20, No. 9, 1997, pp. 1751-1754.

[28] Wertz, J.R., and Larson, W.J. eds., "Space Mission Analysis and Design," Microcosm Press & Kluwar Academic Publishers, El Segundo, CA, 1999, pp. 1-985.

[29] Aguero, V.M., "A Study of Electrical Charging on Large LEO Spacecraft Using a Tethered Satellite as a Remote Plasma Reference," *Stanford University, Space, Telecommunications and Radioscience Laboratory*, 1996, pp. 1-192.

[30] Morris, D., Gilchrist, B., and Gallimore, A., "Integration of Field Emitter Arrays into Spacecraft Systems," *Space Technology and Applications International Forum*, AIAA, 2002, pp. 393-400.

[31] Morris, D., "Optimizing Space-Charge Limits of Electron Emission Into Plasmas in space Electric Propulsion," *University of Michigan*, 2005, pp. 1-212.

[32] Morris, D., and Gilchrist, B., "Electron Field Emission and the Space Charge Limit: Techniques and Tradeoffs," *Joint Propulsion Conference*, AIAA, 2003, pp. 1-9.

[33] Johnson, L., Lorenzini, E., Gilchrist, B.E., "Propulsive Small Expendable Deployer System (ProSEDS) Experiment Mission Overview & Status," *39th AIAA/ASME/SAE/ASEE Joint Propulsion Conference and Exhibit*, AIAA, 2003, pp. 1-9.

[34] Dobrowolny, M., and Stone, N.H., "A Tecnical Overview of TSS-1: the First Tethered-Satellite System Mission," *Il Nuovo Cimento Della Societa Italiana Di Fisica*, Vol. 17C, No. 1, 1994, pp. 1-12.

[35] Hoyt, R.P., "Hoyt Tether Resistance," *Personal Communication*, 2006, pp. 1.

[36] Hoyt, R.P., Slostad, J.T., and Frank, S.S., "A Modular Momentum Exchange Electrodynamic Reboost Tether System Architecture," *39th AIAA/ASME/SAE/ASEE Joint Propulsion Conference and Exhibit*, AIAA, 2003, pp. 1-12.

[37] Forward, R.L., and Hoyt, R.P., "Failsafe multiline Hoytether lifetimes," *31st AIAA, ASME, SAE, and ASEE, Joint Propulsion Conference and Exhibit,* AIAA, 1995, pp. 1-10.

[38] Katz, I., Lilley, J. R. Jr., Greb, A., "Plasma Turbulence Enhanced Current Collection: Results from the Plasma Motor Generator Electrodynamic Tether Flight," *Journal of Geophysical Research,* Vol. 100, No. A2, 1995, pp. 1687-1690.

[39] Bilitza, D., "International Reference Ionosphere 2000," *Radio Science,* Vol. 36, No. 2, 2001, pp. 261-275.

[40] Bilitza, D., "International Reference Ionosphere - Status 1995/96," *Advanced Space Research,* Vol. 20, No. 9, 1997, pp. 1751-1754.

[41] Vas, I.E., Kelly, T.J., and Scarl, E.A., "Space Station Reboost with Electrodynamic Tethers," *Journal of Spacecraft and Rockets,* Vol. 37, No. 2, 2000, pp. 154-164.

[42] Gunther, K., "Hollow Cathode / Ion Source Quotation," HeatWave Labs, Inc., 3968, Watsonville, CA, 2006.

[43] Johnson, L., Carroll, J., Estes, R.D., "Electrodynamic tethers for reboost of the International Space Station and spacecraft propulsion," *AIAA, Space Programs and Technologies Conference,* AIAA, Huntsville, AL, 1996, pp. 1-8.

[44] Choiniere, E., "Analysis of high-voltage cylindrical sheaths in ionospheric plasmas using KiPS-1D and KiPS-2D," *unpublished IEEE Transactions in Plasma Science,* 2004, pp. 1-74.

[45] Fuhrhop, K.R.P., Gilchrist, B.E., "A Comparison of Laboratory Experimental and Theoretical Results for Electrodynamic Tether Electron Collection Performance for Some Bare Tether Geometries," *AIAA SPACE 2009 Conference & Exposition,* AIAA, 2009, pp. 1-10.

[46] Johnson, L., and Herrmann, M., "International Space Station Electrodynamic Tether Reboost Study," NASA, TM--1998-208538, 1998.

[47] Ferguson, D.C., "vxB Effects on Space Station," *2nd International Energy Conversion Engineering Conference,* AIAA, 2004, pp. 1-7.

[48] Singh, N., "Electromagnetic Effects Induced by the Space Station," *Proceedings., Twenty-First Southeastern Symposium on System Theory,* IEEE, 1989, pp. 362-366.

[49] Gilchrist, B.E., Lim, B., Meckel, N., "The use of Electrodynamic Tethers for Orbit Maintenence and Deorbit of Large Spacecraft- A Trade Study of the NASA GLAST Mission," *38th AIAA/ASME/SAE/ASEE Joint Propulsion Conference & Exhibit,* AIAA, 2002, pp. 1-13.